



OPEN ACCESS

Original research

# GLRA2 gene mutations cause high myopia in humans and mice

Qi Tian <sup>1,2,3</sup>, Ping Tong,<sup>4</sup> Gong Chen,<sup>2,3,5,6</sup> Meichun Deng,<sup>2,3,5,6</sup> Tian'e Cai,<sup>7</sup> Runyi Tian,<sup>1,2,3</sup> Zimin Zhang,<sup>1,2,3</sup> Kun Xia,<sup>1,2,3</sup> Zhengmao Hu <sup>1,2,3</sup>

► Additional supplemental material is published online only. To view, please visit the journal online (<http://dx.doi.org/10.1136/jmedgenet-2022-108425>).

For numbered affiliations see end of article.

## Correspondence to

Professor Zhengmao Hu and Professor Kun Xia, Center for Medical Genetics, School of Life Sciences, Central South University, Changsha, Hunan, People's Republic of China; [huzhengmao@sklmg.edu.cn](mailto:huzhengmao@sklmg.edu.cn), [xiakun@sklmg.edu.cn](mailto:xiakun@sklmg.edu.cn) and Dr Ping Tong, Department of Ophthalmology, The Second Xiangya Hospital, Central South University, Changsha, Hunan, People's Republic of China; [tongping@csu.edu.cn](mailto:tongping@csu.edu.cn)

Received 4 January 2022  
Accepted 16 March 2022  
Published Online First 8 April 2022

## ABSTRACT

**Background** High myopia (HM) is a leading cause of blindness that has a strong genetic predisposition. However, its genetic and pathogenic mechanisms remain largely unknown. Thus, this study aims to determine the genetic profile of individuals from two large Chinese families with HM and 200 patients with familial/sporadic HM. We also explored the pathogenic mechanism of HM using HEK293 cells and a mouse model.

**Methods** The participants underwent genome-wide linkage analysis and exome sequencing. Visual acuity, electroretinogram response, refractive error, optical parameters and retinal rod cell genesis were measured in knockout mice. Immunofluorescent staining, biotin-labelled membrane protein isolation and electrophysiological characterisation were conducted in cells transfected with overexpression plasmids.

**Results** A novel HM locus on Xp22.2-p11.4 was identified. Variant c.539C>T (p.Pro180Leu) in *GLRA2* gene was co-segregated with HM in the two families. Another variant, c.458G>A (p.Arg153Gln), was identified in a sporadic sample. The *Gla2* knockout mice showed myopia-related phenotypes, decreased electroretinogram responses and impaired retinal rod cell genesis. Variants c.458G>A and c.539C>T altered the localisation of GlyR $\alpha$ 2 on the cell membrane and decreased agonist sensitivity.

**Conclusion** *GLRA2* was identified as a novel HM-causing gene. Its variants would cause HM through altered visual experience by impairing photoperception and visual transmission.

## INTRODUCTION

Refractive error (RE) is the leading cause of moderate and severe visual impairment and the seventh most prevalent clinical condition globally.<sup>1–3</sup> Four common types of RE are hyperopia, myopia, astigmatism and presbyopia, but myopia is the dominant RE form.<sup>2,3</sup> Currently, there is no internationally agreed quantitative threshold for HM. WHO indicates the threshold for HM of RE  $\leq -5.00$  diopters (D),<sup>4</sup> and the International Myopia Institute (IMI) define the HM as RE below  $-6.00$  D when ocular accommodation is relaxed.<sup>5</sup> HM is a progressive disorder that begins in early childhood and worsens overtime, even after adulthood.<sup>6</sup> HM can be accompanied by elongated axial length, lacquer cracks, retinal atrophy, macular holes and neovascularisation, etc, and it is one of the leading causes of blindness.<sup>7</sup> Myopia and HM rates are predicted to reach 49.8% and 9.8%,

## Key messages

### What is already known on this topic

⇒ High myopia is one of the leading causes of blindness with high global prevalence; however, the genetic and pathogenic basis of high myopia remains largely unknown.

### What this study adds

⇒ This study identifies a novel high myopia causal gene, *GLRA2*, encoding the glycine-gated chloride channel subunit GlyR $\alpha$ 2.  
⇒ Mouse-model study reveals that GlyR $\alpha$ 2 plays a role in vision transmission and rod cell genesis *in vivo*.

### How this study might affect research, practice and/or policy

⇒ This study provides confidential evidence for the conception that abnormal visual experience is a driver for high myopia and chloride channel is involved, further benefiting the genetic counselling, precise intervention and control of high myopia progression.

respectively, worldwide by 2050.<sup>8</sup> According to the twin study, the hereditary of myopia varies from 50% to 90%.<sup>9–10</sup> To date, next-generation sequencing and genome-wide linkage analysis have identified 25 HM loci, and 16 causal genes.<sup>11–12</sup> Moreover, genome-wide association studies and other association studies have uncovered approximately 200 myopia-associated loci. However, these genetic factors can explain only a minority of HM cases, despite its high prevalence in humans.<sup>13</sup>

The eye is an elastic organ that is enveloped by an extracellular matrix (ECM)-rich structure called sclera and looks like a ball in the presence of intraocular pressure (IOP).<sup>14</sup> Abnormal development of the eye and ECM are the two widely accepted factors causing HM.<sup>15–18</sup> On the one hand, the genetic or environmental effectors cause uncontrolled eye enlargement during early development, ultimately leading to HM after birth.<sup>17–19</sup> On the other hand, the intrinsic and extrinsic factors that cause abnormal ECM synthesis and catalysis increase the elasticity and decrease the tension of the sclera.<sup>16</sup> Under these conditions, IOP enlarges the eye resulting in HM.<sup>11–16–18</sup> However, these mechanisms cannot explain the large number of patients with HM. Recently, increasing evidence has emerged to support the idea that HM can be



© Author(s) (or their employer(s)) 2023. Re-use permitted under CC BY-NC. No commercial re-use. See rights and permissions. Published by BMJ.

**To cite:** Tian Q, Tong P, Chen G, *et al.* *J Med Genet* 2023;**60**:193–203.

a visually driven abnormality.<sup>20,21</sup> Genetics studies have shown that many HM-related genes, such as *OPN1LW*,<sup>22</sup> *RDH5*<sup>12</sup> and *NYX*,<sup>23</sup> are associated with photopic perception, retinal circuit and visual transmission. These findings indicate that impaired visual experience, mainly composed of photoperception and visual information transmission, may play a vital role in HM onset and development.<sup>12,15,20</sup> Emmetropisation is a vision-dependent process that controls the development of RE and eye growth.<sup>24</sup> Gene mutations that cause impaired visual experience may result in overemmetropisation and uncontrolled eyeball growth, thereby leading to HM.<sup>12,25</sup>

Thus, we aimed to explore the genetic mechanisms of HM by studying 38 individuals (composed of 18 patients and 20 normal subjects) from two unrelated Chinese families with HM and 200 patients with familial/sporadic HM. Using genome-wide linkage analysis combined with exome sequencing (ES) and Sanger sequencing screening, we identified two HM-related variants in *GLRA2* gene (GenBank: NM\_002063.4, NP\_002054.1): c.458G>A (p.Arg153Gln) and c.539C>T (p.Pro180Leu). Moreover, we constructed knockout mice using the CRISPR/Cas9 system and analysed their myopic phenotypes, retinal morphology and rod cell differentiation to elucidate the mechanism of HM pathogenesis.

## METHODS

### Subjects and clinical examination

This study recruited individuals from two unrelated families with HM (HM1 and HM2) and 200 patients with familial/sporadic HM from the Chinese population. HM1 and HM2 families included 8 and 10 patients with HM, respectively, and 10 asymptomatic subjects each family. Among the 200 patients with familial/sporadic HM recruited, the gender ratio was 79:121 (male:female). In adult subjects, HM was defined using the WHO recommended threshold as RE  $\leq -5.00$  D in either eye.<sup>5</sup> Subjects younger than 15 years with moderate myopia ( $-3.00$  D  $\leq$  RE  $< -5.00$  D) were also considered as patients with HM.

All ophthalmological examinations were performed at the Second Xiangya Hospital, Central South University. Visual acuity and refraction were measured using a LogMAR chart and autorefractor (Huvitz HRK-1 Autorefractor, Coburn Technologies, Singapore), respectively. The lens and vitreous were measured using a slit lamp (Huvitz Slit Lamp HS-5000, Coburn Technologies, Singapore), retina using an ophthalmoscope (NTZ-OPH-BXa-RC Neitz Ophthalmoscope, Neitz Instruments, Japan) and axial length using an A-scan ultrasound device (ABSolu A/B/S/UBM Ultrasound Platform, Quantel Medical, France).

### Genome-wide linkage analysis and haplotyping

Eighteen samples from the HM1 family were genotyped using Illumina iScan system (Illumina, USA) and Illumina HumanCytoSNP-12 V.2.1 BeadChip kit. Genotypes were called and quality controlled using Illumina GenomeStudio 2011. Genome-wide linkage disequilibrium of HM1 family was tested by merlin V.1.1.2<sup>26</sup> under multiple-parameter analysis with 'High\_myopia 0.001 0.001,0.9,0.99 rare\_dominant' settings. The 'merlin' or 'minx' prompt was used to analyse the autosomal or X linked linkage disequilibrium separately. Merlin V.1.1.2 drew the haplotype of HM1 and HM2 families with the 'best' option.

### Exome sequencing

The gDNA of HM1-I:2, HM1-II:4, HM1-III:10, HM2-III:4, HM2-IV:5 and HM2-IV:6 were analysed through ES as previously described.<sup>27</sup> Briefly, the library was captured using Agilent

SureSelectXT Human All Exon V4+UTRs probe and sequenced on Illumina HiSeq 2000 sequencing system (Illumina) with PE100. The reads were then aligned to the human genome assembly GRCh37/hg19 using bwa 0.7.10.<sup>28</sup> Variants were called with GATK 3.2.2<sup>29</sup> and annotated using ANNOVAR.<sup>30</sup>

After screening out variants with allele frequency  $>0.01$  in the gnomAD (<https://gnomad.broadinstitute.org/>) and 1000 Genomes Project (<https://www.internationalgenome.org/>) databases, all patients shared non-synonymous variants (including single nucleotide variants (SNVs) and insertion-deletion polymorphisms (indels)) in the consensus coding sequence (CCDS), and the canonical splicing sites were reserved. Variants within the linkage region were selected for co-segregation analysis.

### Primer design and co-segregation analysis of the candidate variants

All primers were designed using the online software Primer3 (<https://primer3.ut.ee/>) based on the human GRCh37/hg19 or mouse GRCm38/mm10 assemblies (online supplemental table 1). PCR and Sanger sequencing were performed to confirm the co-segregation status of the candidate variants in the samples of HM families and to screen for gene variants in the samples of patients with familial/sporadic HM.

### Visual acuity and refractive error evaluation of *Gla2* knockout mice

*Gla2* knockout mice were developed by zygote injection of CRISPR/Cas9 mRNA and a pair of gRNAs flanking the second exon of *Gla2* gene (GenBank: NM\_183427.5), which was shared by all isoforms. It was predicted that the deletion of this exon would cause a frameshift during *Gla2* mRNA translation. Knockout efficiency was validated using RT-PCR and Sanger sequencing of the mRNA extracted from the retina of adult knockout mice. All the animals evaluated were male. Visual acuity was assessed under 100 lux light intensity following the protocol by Prusky *et al.*<sup>31</sup> RE was measured using an eccentric infrared photorefractor (custom built) according to the method by Schaeffel *et al.*<sup>32</sup>

### Ocular biometry measuring and electroretinography recording

The ocular biometry of *Gla2* knockout mice, including corneal radius, corneal thickness, chamber depth, lens thickness, vitreous depth, retinal thickness and axial length, was measured using optical coherence tomography (OCT) following the protocol by Zhou (custom built).<sup>33</sup> Electroretinography (ERG) recording was performed using a six-step workflow following the modified instructions of the International Society for Clinical Electrophysiology of Vision. Briefly, mice were dark-adapted for at least 4 hours and anaesthetised by the intraperitoneal administration of ketamine and xylazine mixture. The pupils were then dilated with compound tropicamide eye drops and the electrodes were placed at their corresponding positions. Dark-adapted scotopic 0.01, scotopic 3.0, scotopic 10.0 and oscillatory potentials (OPs) were recorded sequentially using a RETI-port/scan 21 system (Q450SCX, Roland Consult, Germany). After 2 min of light adaptation, photopic 3.0 and photopic 3.0 flicker 30 Hz responses were recorded.

### Immunohistofluorescence and H&E staining of mouse retina

Paraffin-embedded mice eyeballs were sagittally sectioned into 4  $\mu$ m slices using paraffin microtome (RM2235, Leica Biosystems,

Germany). Paraffin sections were dewaxed and rehydrated and permeated with 0.1% Triton-X in 1× phosphate-buffered saline (PBS) at room temperature. The sections were then blocked with 5% bovine serum albumin (BSA) in 1× PBS containing 0.3M glycine and incubated overnight with a primary antibody diluted with 5% BSA in 1× PBS at 4°C. After incubation with a fluorescent-conjugated second antibody and the nuclear staining with 4',6-Diamidino-2-phenylindole dihydrochloride (DAPI), the sections were mounted and captured using a confocal microscope (Leica TCS SP5, Leica Biosystems). The primary antibody used was anti-rhodopsin (Cat: ab98887, Abcam, USA).

OCT-embedded eyeballs were sagittally sectioned into 14µm slices using a cryostat microtome (CM1850, Leica Biosystems). OCT-embedded sections were postfixed with 4%

paraformaldehyde (PFA) and stained using an H&E staining kit according to the manufacturer's instructions (Cat: ab245880, Abcam).

**Cell culture and immunofluorescent staining**

HEK293 cell line (American Type Culture Collection) was cultured in high-glucose Dulbecco's Modified Eagle Medium containing 10% fetal bovine serum (FBS) and transfected with wild-type (WT), GLRA2<sup>R153Q</sup>, GLRA2<sup>P180L</sup> and GLRA2<sup>V341I</sup> overexpression plasmids using Lipofectamine 2000 reagent (Cat: 11668030, Thermo Scientific, USA).

The retina of P5.5 age mice were dissected and dissociated using papain and DNase I. The resuspended cells were cultured in

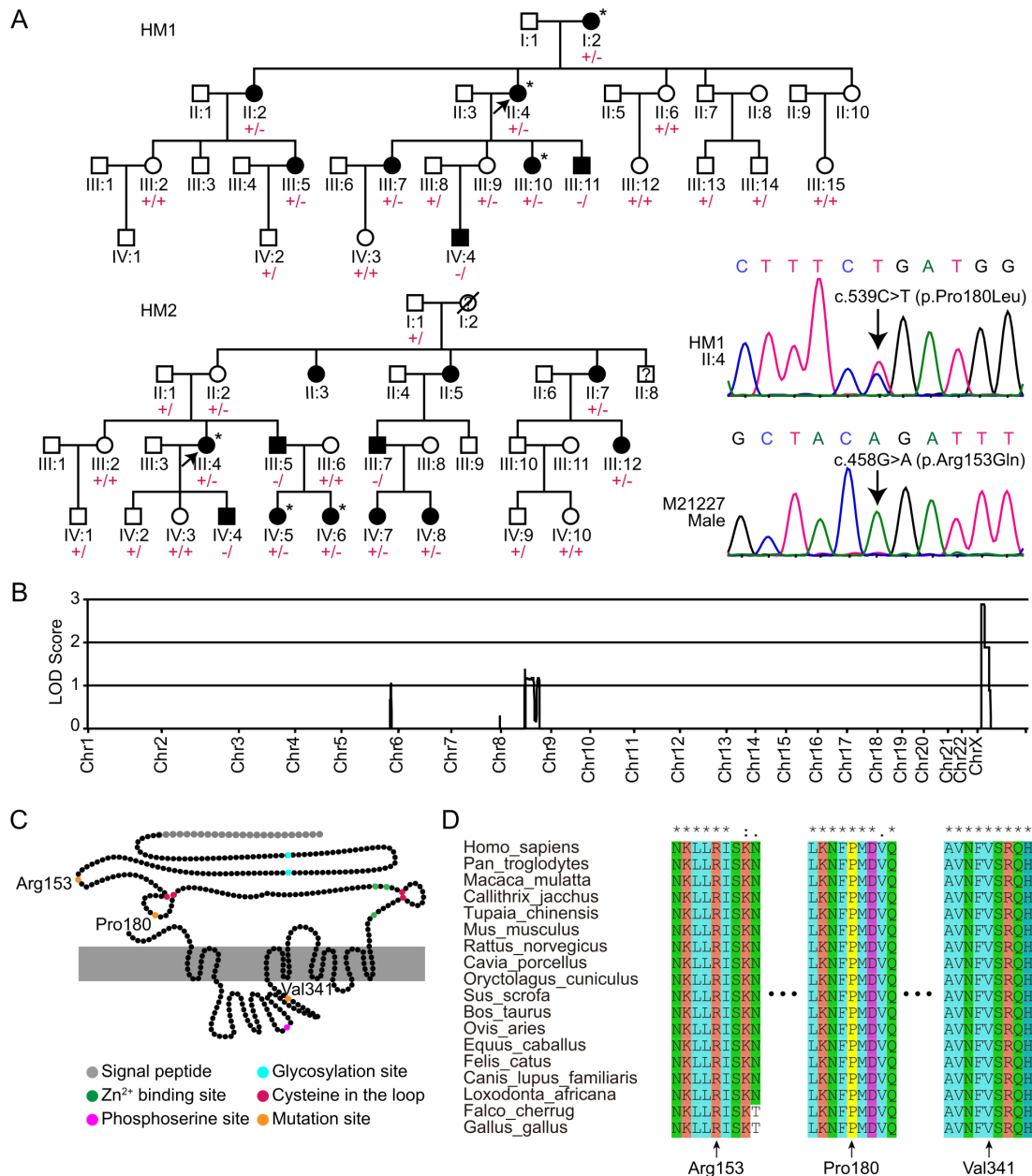


**Figure 1** Genetic studies of high myopia (HM) families and sporadic patients. (A) Pedigree of two HM families and Sanger sequencing of c.458G>A (p.Arg153Gln) and c.539C>T (p.Pro180Leu) variants in *GLRA2* gene. (B) Genome-wide multipoint linkage analysis of HM1 family. (C) Schematic structure of GlyRα2 and three missense variant's locations. (D) Amino acid conservation alignment of Arg153, Pro180 and Val341. The arrow in the pedigree indicates the proband. '□' and '○' symbols present asymptomatic male and female subjects, respectively; '■' and '●' characters stand for male and female patients, respectively. Samples selected for exome sequencing (ES) were marked with '\*'. '+' stands for wild-type allele and '-' refers to c.539C>T allele.

**Table 1** Clinical characteristics in HM1 family

ID	Sex	Age (years)	Status	Refraction (D)		Axial length (mm)		Fundus	Genotype
				Ocular Dexter (OD)	Oculus Sinister (OS)	OD	OS		
I:2	F	80–85	Patient	−14.00	−14.00	29.12	28.09	Retinal atrophy	c.539C>T, Het
II:2	F	60–65	Patient	−15.00	−10.00	29.34	27.61	Bilateral tigroid fundus	c.539C>T, Het
II:4	F	55–60	Patient	−15.00	−15.00	29.94	29.73	Bilateral tigroid fundus, retinal atrophy	c.539C>T, Het
II:6	F	55–60	Normal	Plano	Plano	NA	NA	NA	WT
III:2	F	35–40	Normal	−2.50	−2.50	NA	NA	NA	WT
III:5	F	30–35	Patient	−12.00*	−12.00	27.38	28.08	Bilateral tigroid fundus	c.539C>T, Het
III:7	F	35–40	Patient	−6.00*	−6.00	NA	NA	NA	c.539C>T, Het
III:8	M	35–40	Normal	−1.00	−1.00	NA	NA	NA	WT
III:9	F	30–35	Normal	−0.50	0.00	23.59	23.46	Normal	c.539C>T, Het
III:10	F	30–35	Patient	−5.75	−5.50	24.75	24.77	NA	c.539C>T, Het
III:11	M	25–30	Patient	−8.00	−8.00	26.46	26.19	Normal	c.539C>T, Hemi
III:12	F	25–30	Normal	−2.00	−2.00	NA	NA	NA	WT
III:13	M	15–20	Normal	Plano	Plano	NA	NA	NA	WT
III:14	M	10–15	Normal	−1.50	+2.00	26.02	24.16	Normal	WT
III:15	F	15–20	Normal	Plano	Plano	NA	NA	NA	WT
IV:2	M	5–10	Normal	Plano	Plano	NA	NA	NA	WT
IV:3	F	5–10	Normal	Plano	Plano	NA	NA	NA	WT
IV:4	M	5–10	Patient	−9.00	−9.00	27.48	27.26	Bilateral tigroid fundus, retinal atrophy	c.539C>T, Hemi

\*LASIK eye surgery 10 years before.

F, female; Hemi, hemizygote; Het, heterozygote; M, male; NA, not applicable; WT, wild-type.

a Lab-Tek Chamber with minimum essential medium containing 10% FBS.

The HEK293 and retina cells were washed with 1× PBS, fixed with 4% PFA, and then permeated with 0.1% Triton-X in 1× PBS or non-permeated with 1× PBS at room temperature. The cells were stained with the same procedures used for immunohistofluorescence (IHF) staining. The primary antibodies used were anti-GlyRα2 (Cat: ab97628, Abcam) and anti-rhodopsin (Cat: ab98887, Abcam).

### Detection of biotin-labelled membrane proteins of transfected HEK293 cells

Membrane proteins were biotinylated following the manual instructions of the EZ-Link Sulfo-NHS-LC-Biotinylation kit (Cat: 21435, Thermo Scientific). For western blot analysis detection, the samples were separated on a 12% sodium dodecyl sulfate-polyacrylamide gel electrophoresis and transferred to a polyvinylidene fluoride membrane. The membranes were incubated with a primary antibody overnight at 4°C. The primary antibodies used were anti-GlyRα2 (Cat: ab97628, Abcam), anti-E-cadherin (Cat: ab15148, Abcam) and anti-GAPDH (Cat: ab9484, Abcam). Next, the horseradish peroxidase-conjugated secondary antibody was incubated for 1 hour at room temperature, and the bands were visualised using the ECL substrate.

### Electrophysiology experiment

After HEK293 cells were transfected with overexpression plasmids, the whole-cell currents were recorded using the HEKA EPC9 system (Harvard Bioscience, USA) under voltage-clamp mode at −60 mV at 25°C±1°C. The patch-pipette resistance was approximately 1–3 MΩ when filled with intracellular buffer, and the glycine solutions (0.01 mM to 1 M) were applied by the ‘U’ tube incubation system. Extracellular buffer: NaCl 140.0 mM, KCl 5.0 mM, CaCl<sub>2</sub> 2.0 mM, MgCl<sub>2</sub> 1.0 mM, N-2-hydroxyethylpiperazine-N-ethane-sulphonic acid (HEPES) 10.0

mM, D-glucose 10.0 mM; pH adjusted to 7.4 with NaOH. Intracellular buffer: CsCl 145.0 mM, MgATP 2.0 mM, CaCl<sub>2</sub> 2.0 mM, MgCl<sub>2</sub> 2.0 mM, ethylene glycol tetraacetic acid 10.0 mM, HEPES 10.0 mM; pH adjusted to 7.4 with caesium hydroxide. Normalised concentration-response curves were fitted using the following equation:

$$I/I_{max} = 1/(1 + (EC50/[glycine])^H)$$

where I/I<sub>max</sub> is the normalised current amplitude, EC50 is the glycine concentration that evokes half of the maximal response and H is the Hill coefficient.

### Statistics analysis

The statistical significance of the differences in the OPs, photopic a and b wave, photopic 3.0 flicker 30Hz amplitude, normalised ocular parameters, retinal layer thickness, visual acuity, and RE between *Gtra2* knockout and WT mice was determined using paired t-test with a two-tailed p-value. A two-way analysis of variance was used to assess the difference in dark-adapted ERG a-wave and b-wave amplitude between *Gtra2* knockout and WT mice. The dose-normalised response was non-linearly regressed using a variable slope. Statistical significance was set at p≤0.05.

## RESULTS

### Clinical characteristics

In HM1 family, patients with HM (figure 1A and table 1) presented eye RE ranging from −15.00 to −5.50 D. Fundus photography revealed that patients II:2, II:4, III:5 and IV:4 with bilateral tigroid fundus; patients I:2, II:4 and IV:4 with retinal atrophy (figure 2). Moreover, patient III:11 presented a decreased dark-adapted ERG response to the scotopic 0.01 b, scotopic 3.0 a and b and OP waves (figure 2A,B). In HM2 family, patients with HM (figure 1A and table 2) presented eye RE ranging from −11.00 to −3.25 D. Among the 200 patients with

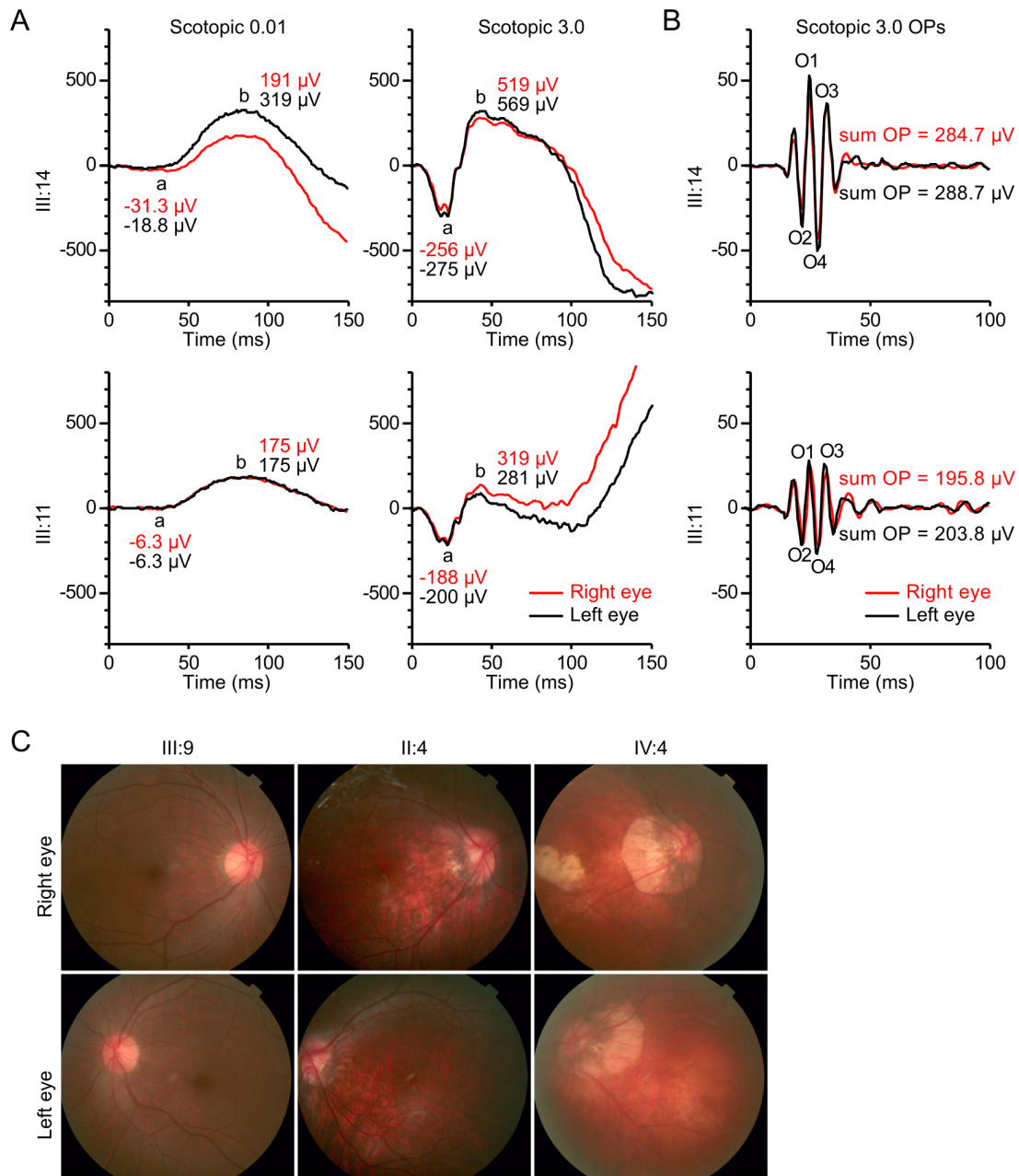


**Figure 2** Clinical features of patients in HM1 family. (A) Dark-adapted electroretinography results of asymptomatic subject III:14 and patient III:11. (B) Fundus of asymptomatic subject III:9, female patient II:4 and male patient IV:4. HM, high myopia; OP, oscillatory potential.

familial/sporadic HM recruited, eye RE ranged from  $-33.00$  to  $-5.50$  D.

#### c.539C>T (p.Pro180Leu) variant in *GLRA2* gene co-segregated with high myopia

In HM1 family, all subjects participated in linkage analysis. As IV:4 was highly myopic, we proposed his mother III:9 should be an obligate carrier. Parametric multipoint linkage analysis of HM1 family showed no known HM locus throughout the genome. On auto-chromosome, two regions, 5q33.3-q34 and 8q21.12-q24.13, with a maximum logarithm of odds (LOD) score of only 1.008 and 1.39, respectively were identified. In addition, we identified a novel highly linked locus of approximately 24.7 Mb on Xp22.2-p11.4, with a maximum LOD score of 2.88, surrounding the marker rs4825340 (figure 1B and

online supplemental table 2). No known HM causal genes were found in this linkage region.

Through ES of patients I:2, II:4 and III:10 from HM1 family, we harvested 12.6, 11.4 and 11.3 Gb raw data with mean depth of 128, 118 and 121, respectively. We identified 35 483 combined variants (including SNVs and indels) with a frequency below 0.5 in the 1000 Genomes Project by annotation. Finally, we got 1192 shared non-synonymous variants within the CCDS and canonical splicing sites with a frequency lower than 0.01 in the gnomAD\_Genome\_asn, gnomAD\_ExAc\_asn and maf1000g\_asn databases. No mutations were identified in the known HM-causing genes.

Genome-wide linkage analysis, ES and Sanger sequencing revealed that only the rare non-synonymous variant in the linkage loci, *GLRA2*: c.539C>T (p.Pro180Leu), was co-segregated with

**Table 2** Clinical characteristics in HM2 family and sporadic HM patient M21227

ID	Sex	Age	Status	Refraction (D)		Axial length (mm)		Genotype
				OD	OS	OD	OS	
HM2-I:1	M	85–90	Normal	Plano	Plano	NA	NA	WT
HM2-II:1	M	60–65	Normal	Plano	Plano	NA	NA	WT
HM2-II:2	F	60–65	Normal	Plano	Plano	NA	NA	c.539C>T, Het
HM2-II:7	F	55–60	Patient	−10.00	−10.00	NA	NA	c.539C>T, Het
HM2-III:2	F	35–40	Normal	Plano	Plano	NA	NA	WT
HM2-III:4	F	35–40	Patient	−9.00	−9.00	26.2	26.07	c.539C>T, Het
HM2-III:5	M	35–40	Patient	−7.50	−6.50	23.71	23.76	c.539C>T, Hemi
HM2-III:6	F	35–40	Normal	Plano	Plano	NA	NA	WT
HM2-III:7	M	35–40	Patient	−6.00	−6.00	NA	NA	c.539C>T, Hemi
HM2-III:12	F	10–15	Patient	−4.00*	−4.00	NA	NA	c.539C>T, Het
HM2-IV:1	M	5–10	Normal	Plano	Plano	NA	NA	WT
HM2-IV:2	M	15–20	Normal	Plano	Plano	NA	NA	WT
HM2-IV:3	F	10–15	Normal	Plano	Plano	NA	NA	WT
HM2-IV:4	M	5–10	Patient	−3.25*	−3.75	23.62	23.74	c.539C>T, Hemi
HM2-IV:5	F	5–10	Patient	−8.00	−11.00	25.27	26.19	c.539C>T, Het
HM2-IV:6	F	1–5	Patient	−9.50	−10.00	26.11	26.28	c.539C>T, Het
HM2-IV:7	F	10–15	Patient	−9.50	−6.75	26.23	25.00	c.539C>T, Het
HM2-IV:8	F	5–10	Patient	−7.75	−9.00	26.32	26.72	c.539C>T, Het
HM2-IV:9	M	5–10	Normal	Plano	Plano	NA	NA	WT
HM2-IV:10	F	1–5	Normal	NA	NA	NA	NA	WT
M21227	M	10–15	Patient	−13.00	−13.50	28.3	28.17	c.458G>A, Hemi

\*Moderate phenotype due to young age.

F, female; Hemi, hemizygote; Het, heterozygote; M, male; NA, not applicable; WT, wild-type.

the HM phenotype in HM1 family, and that III:9 was heterozygote (figure 1A). ES and Sanger sequencing data indicate that the c.539C>T variant was also co-segregated with HM phenotype in HM2 family (figure 1A and table 2). Moreover, II:2 was a heterozygote and had normal vision. The haplotypes of the ES samples with the c.539C>T variant were then included to determine whether the variant was located on the same haplotype in both families. We found that HM1 and HM2 families had different haplotypes from rs3764879 through c.539C>T to rs2229137, suggesting no founder effect (online supplemental figure 1A).

Two additional rare variants were identified by screening *GLRA2* gene in the 200 unrelated patients with familial/sporadic HM: c.458G>A (p.Arg153Gln) in sporadic sample M21227 and c.1021G>A (p.Val341Ile) in IV:1 from HM3 family. Sanger sequencing results showed that c.1021G>A variant descended from II:3 and III:2 which were emmetropic. Variant c.1021G>A did not co-segregate with HM phenotype in HM3 family (online supplemental figure 1B). Therefore, variant c.1021G>A may be a polymorphism.

### *Gla2* knockout mice had myopic phenotypes

To further confirm the relationship between *GLRA2* gene and HM, a *Gla2* knockout mouse model was used. Detailed inspection revealed that *Gla2* knockout mice had regular overall postnatal developments and that each individual was born at a Mendelian ratio without morphological abnormalities. *Gla2* knockout mice also behaved normally, so did their WT littermates.

We evaluated the visual acuity of *Gla2* knockout mice with a modified Y-maze according to the methods by Prusky *et al.*<sup>31</sup> After two training days, all mice passed the test criterion with >80% correction rates in 20–40 sequential trials. This result demonstrated that *Gla2* knockout mice had regular

learning and motor abilities. Nevertheless, the visual acuity of *Gla2* knockout mice was worse than that of their WT littermates (knockout: 0.55 cycles per degree (cpd) vs WT: 0.60 cpd,  $p < 0.05$ ,  $n = 11$  pairs) (figure 3A). We measured the mice RE according to the protocol by Schaeffel *et al.*<sup>32</sup> Under dark adaptation, *Gla2* knockout mice had regular pupil size (knockout:  $2.52 \pm 0.04$  mm, WT:  $2.47 \pm 0.06$  mm,  $p > 0.05$ ,  $n = 8$  pairs); however, they were more myopic than WT littermates (knockout:  $-3.92 \pm 1.34$  D, WT:  $-0.50 \pm 0.72$  D,  $p < 0.05$ ,  $n = 8$  pairs) (figure 3B).

### *Gla2* knockout mice had reduced corneal thickness and dark-adapted electroretinography response

OCT experiments were performed to assess the ocular parameters of *Gla2* knockout mice and to determine the origin of RE and visual acuity reduction. OCT results showed that *Gla2* knockout mice had thinner corneas than their WT littermates (knockout:  $0.1167 \pm 0.0037$  mm, WT:  $0.1259 \pm 0.0037$  mm,  $p < 0.05$ ,  $n = 8$  pairs) (figure 3C). Conversely, other parameters such as corneal radius, chamber depth, lens thickness, vitreous depth, retinal thickness and axial length were not altered in *Gla2* knockout mice (online supplemental figure 2A and online supplemental table 3). In addition, the thickness and stratification of the retina was similar in adult knockout and WT mice (online supplemental figure 2B,C).

We evaluated the retinal activity using ERG because *GLRA2* is expressed in the retina and may play a role in the transmission of visual stimuli. After a dark adaptation, *Gla2* knockout mice presented decreased scotopic a and b waves and OPs wave amplitude (figure 3D–E). The photopic results revealed a reduced response to flash stimuli at both a and b and flicker wave amplitudes in knockout mice. However, the differences were not statistically significant (online supplemental figure 2D,E and online

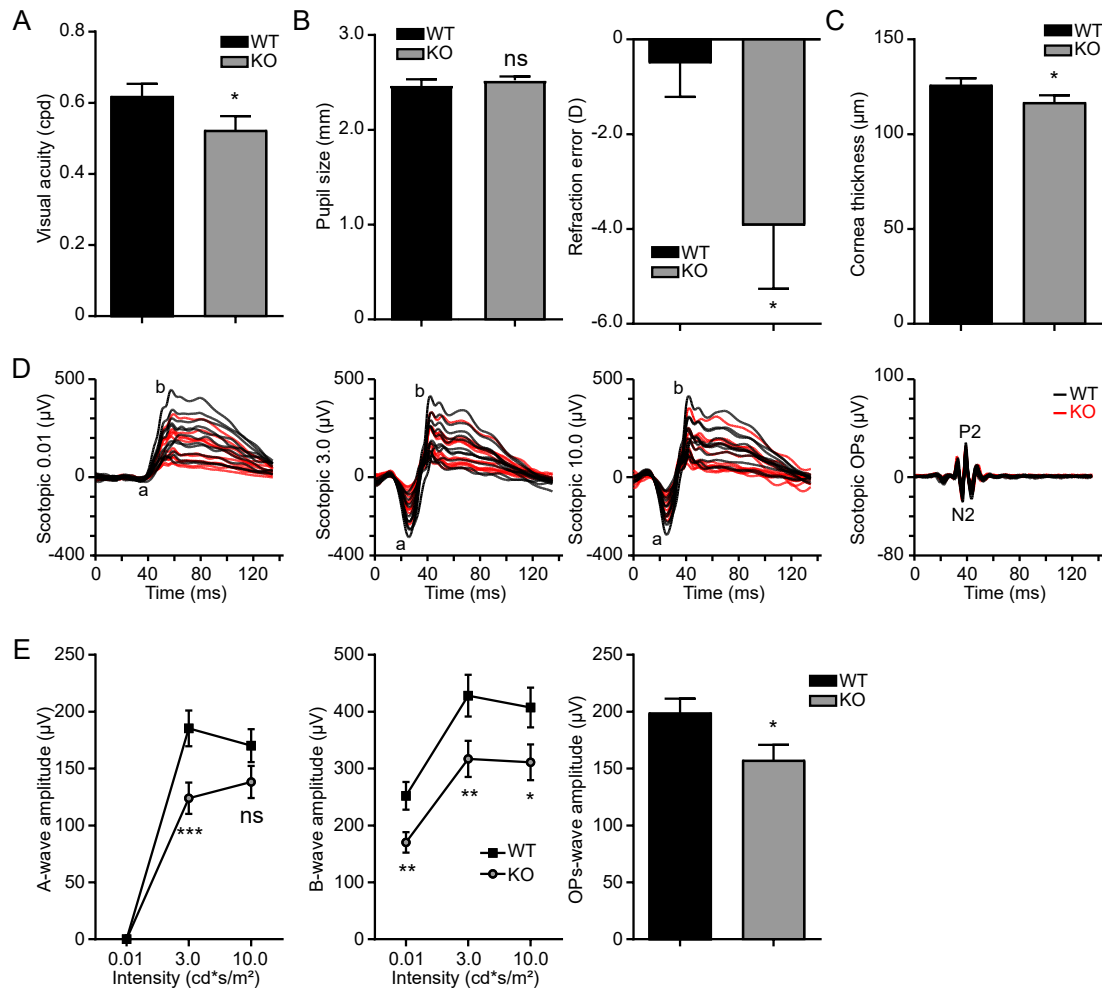


**Figure 3** Myopia-related phenotypes of *Glra2* knockout (KO) mice. (A) Visual acuity of *Glra2* knockout and wild-type (WT) mice. (B) Pupil size and refractive error of *Glra2* KO and WT mice. (C) Normalised central corneal thickness of *Glra2* KO and WT mice. (D) Dark-adapted electroretinography results of *Glra2* KO and WT mice. (E) Statistical results of (D). Data are represented as mean±SEM. ns, not significant; \* $P < 0.05$ ; \*\* $P < 0.01$ .

supplemental table 4). These results revealed a malfunction in rod pathway transduction exclusively in *Glra2* knockout mice.

#### *Glra2* defects hampered the retina rod cell genesis in vivo

We performed IHF assays on the retinas of P5.5 mice to assess rod genesis by staining the rod cell marker, rhodopsin. *Glra2* defects dramatically decreased the rhodopsin-positive staining in the P5.5 mouse retina (figure 4A). To accurately evaluate the changes in cell differentiation, we calculated the proportion of rhodopsin-positive cells in primarily cultured retinal cells derived from P5.5 age mice after immunofluorescent staining with anti-rhodopsin. Rod cell genesis in *Glra2* knockout mice decreased by approximately one-quarter (knockout: 19.32%, 95% CI 18.32% to 20.34%;  $p < 0.001$ ) compared with WT littermates (WT: 25.73%, 95% CI 24.68% to 26.79%) (figure 4B,C).

#### c.458G>A (p.Arg153Gln) and c.539G>T (p.Pro180Leu) variants disrupted GlyR $\alpha$ 2 membrane location and agonist binding affinity

To evaluate the effects of the variants, we transfected HEK293 cells with WT, GLRA2<sup>R153Q</sup>, GLRA2<sup>P180L</sup> and GLRA2<sup>V341I</sup> plasmids. Immunofluorescent results showed that WT and GLRA2<sup>V341I</sup> proteins were expressed and located on the cell membranes with a scattered distribution. However, GLRA2<sup>R153Q</sup> and GLRA2<sup>P180L</sup> proteins were undetectable in the cell membrane

(online supplemental figure 3A). Isolation of biotin-labelled membrane proteins also demonstrated that the membrane localisation of GLRA2<sup>R153Q</sup> and GLRA2<sup>P180L</sup> proteins was disrupted (online supplemental figure 3B).

As GlyR $\alpha$ 2 is a membrane protein of the glycine-gated chloride channel family, we evaluated whether GLRA2<sup>R153Q</sup> and GLRA2<sup>P180L</sup> proteins could alter electrophysiological features through whole-cell patch experiments using HEK293 cells. As expected, the dose-response curves of GLRA2<sup>R153Q</sup> and GLRA2<sup>P180L</sup> shifted rightward compared with those of WT. Moreover, the EC50 value of glycine was significantly higher in GLRA2<sup>R153Q</sup> and GLRA2<sup>P180L</sup> than in WT (GLRA2<sup>R153Q</sup>:  $11.550 \pm 0.666$  mM,  $p < 0.001$ ; GLRA2<sup>P180L</sup>:  $124.000 \pm 11.260$  mM,  $p < 0.001$ ; WT:  $0.083 \pm 0.010$  mM). Meanwhile, GLRA2<sup>V341I</sup> only had a slightly elevated EC50 value ( $0.211 \pm 0.017$  mM,  $p < 0.001$ ) compared with WT (online supplemental figure 3C). GLRA2<sup>R153Q</sup> and GLRA2<sup>P180L</sup> dramatically reduced GlyR $\alpha$ 2 sensitivity to glycine and were unlikely to be activated in response to the physiological concentration of glycine.

#### DISCUSSION

In this study, we identified the pathogenic variant c.539C>T (p.Pro180Leu) in *GLRA2* gene, which co-segregated with HM in two unrelated Chinese families. The haplotype analysis showed

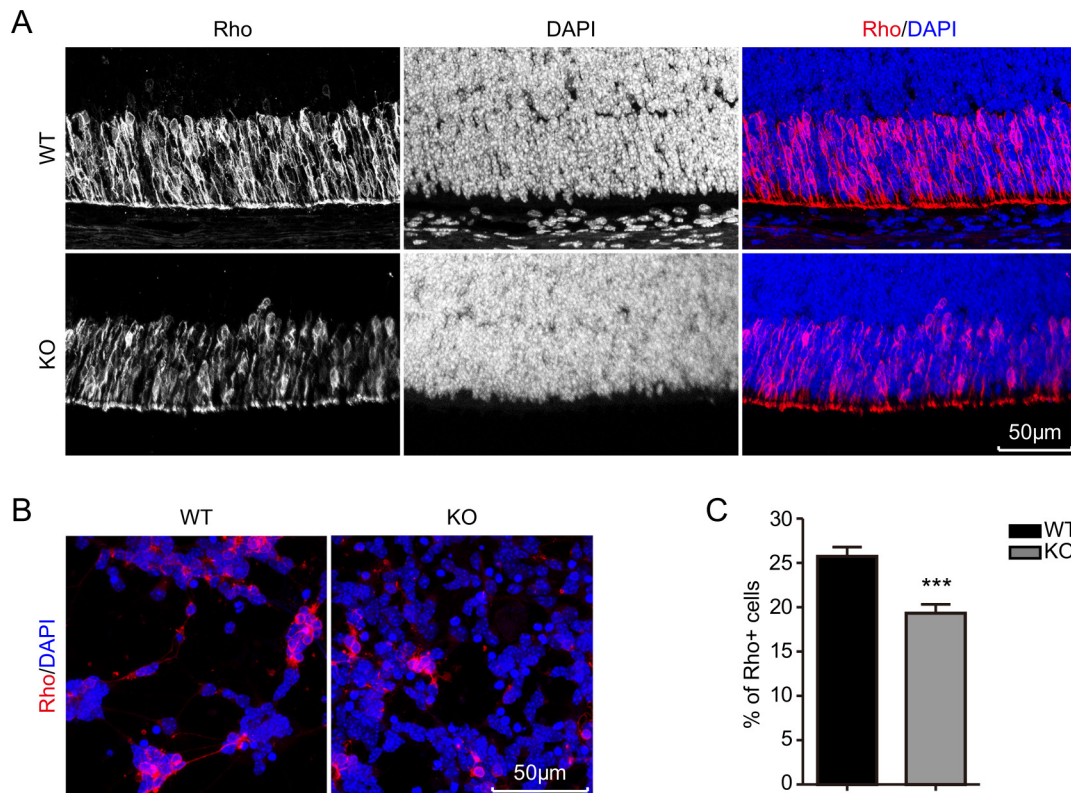


**Figure 4** Immunohistochemistry staining of mouse retina and immunofluorescent staining of primarily cultured retina cells. (A) Retina rod cell genesis in P5.5 age mice of each genotype. Immunohistochemistry staining of paraffin sections from P5.5 age mouse retina; rod cells stained with anti-Rho are shown in red colour, and the nucleus is presented in blue. (B, C) Immunofluorescent staining and statistical results of the primarily cultured cells from P5.5 age mouse retina. Rho: Rhodopsin, a marker of the rod cell. The errors bar presents a 95% CI. \*\*\* $P < 0.001$ .

no founder effects. These results indicated that c.539C>T was mutated separately in HM1 and HM2 families. We also found the pathogenic variant c.458G>A (p.Arg153Gln) in a patient with sporadic HM. In knockout mice, *Gla2* deficiency caused myopia. This is the first evidence showing that *GLRA2* gene can cause HM in humans and mice.

To date, no eye diseases caused by *GLRA2* mutations have been reported.<sup>34,35</sup> *GLRA2* is highly expressed in the CNS and retina<sup>36,37</sup>; it encodes the  $\alpha 2$  subunit of the glycine receptor GlyR $\alpha 2$ , which is a ligand-gated chloride channel. In the adult mouse retina, GlyR $\alpha 2$  can enhance the excitatory centre response through crossover inhibition between the ON and OFF pathways,<sup>38</sup> which is essential for the contrast encoding of visual stimuli.<sup>39</sup> Besides myopia, we recorded the decrease of both dark-adapted ERG responses and corneal thickness in *Gla2* knockout mice. Moreover, we observed hampered rod genesis in the *Gla2* knockout mouse retina, in accordance with findings in vitro by Young and Cepko.<sup>40</sup> GlyR $\alpha 2$  deficiency might cause insufficient photoperception and impaired visual transmission and processing, resulting in an altered visual experience. And the altered visual experience could ultimately lead to HM in both humans and mice.<sup>13,20,41</sup>

Variants c.458G>A (p.Arg153Gln) and c.539C>T (p.Pro180Leu) were absent in the gnomAD database and were highly conserved among many vertebrate animals (figure 1D). Arg153 is located in the first topological domain of GlyR $\alpha 2$  protein, while Pro180 is enveloped in the first cysteine loop domain of GlyR $\alpha 2$  protein (figure 1C). These domains are believed to play a crucial role in the agonist and antagonist binding and electrophysiological response.<sup>42,43</sup> We found that both variants can disrupt the membrane location of GlyR $\alpha 2$ .

GLRA2<sup>R153Q</sup> and GLRA2<sup>P180L</sup> dramatically reduced GlyR $\alpha 2$  sensitivity to glycine, so that it would not be activated by the physiological concentration of glycine. These results indicated that c.458G>A and c.539C>T are pathogenic variants related to HM.

Notably, HM1-III:9 and HM2-II:2 subjects were both heterozygotes, which do not manifest HM. Therefore, the penetrance of the pathogenic variant c.539C>T in *GLRA2* gene is incomplete (2/20), as observed in HM families. As *GLRA2* is located on the X chromosome, we speculated that the incomplete penetrance of variant c.539C>T may be caused by skewed X-inactivation. However, we failed to detect any differences in the inactive proportion of X chromosomes between III:9 and other female patients in HM1 family using genomic DNA from peripheral blood lymphocyte (online supplemental figure 4). Thus, the causes of incomplete penetrance remain to be investigated in more dedicated studies. Moreover, a larger sample size is needed to depict the penetrance of c.539C>T in hemizygotes and the severity between hemizygotes and age-matched female heterozygotes.

Variant c.1021G>A (p.Val341Ile) is located in the topological domain between transmembrane domain 3 (TM3) and TM4 of GlyR $\alpha 2$  (figure 1C). This rare variant was found in the gnomAD database (1.09082e-05). This variant did not co-segregate with HM in HM3 family and did not affect GlyR $\alpha 2$ 's membrane location, but had a slightly increased EC50 value. Considering that the glycine concentration at the synapses is estimated to be in the millimolar range,<sup>44</sup> GLRA2<sup>V341I</sup> may normally respond to the physiological concentration. Therefore, c.1021G>A is not a pathogenic variant related to HM.

Variants in *GLRA2* gene have been associated with autism disorders. Pinto reported an autistic patient with a 151 kb deletion in *GLRA2* gene inherited from his mother. Notably, the patient, his mother, and his maternal grandfather had HM.<sup>35 45</sup> Variant c.458G>A was also identified in an autistic boy (de novo mutation); however, the genotype of his autistic elder sister on this allele was WT.<sup>35</sup> Additionally, three *GLRA2* variants were reported in 2650 patients with autism; two were de novo and one was maternally inherited (online supplemental table 5).<sup>34 35 46 47</sup> In the current study, sporadic and familial patients with *GLRA2* variants exhibited normal social, behavioural and communication skills with personal contact. The phenotype caused by *GLRA2* mutations was non-syndromic HM.

Our study had the following limitations: (1) the number of sporadic patients recruited was not large enough to evaluate the contribution of *GLRA2* mutations to HM; (2) the causes of incomplete penetrance of c.539C>T (p.P180L) in female carriers and whether this phenomenon is common in male hemizygotes are unclear; (3) even though knockout mice showed myopia-related phenotypes, we failed to detect significant differences in axial elongation between *Gla2* knockout and WT mice. According to Schmucker and Schaeffel,<sup>48</sup> the  $-3.4$  D RE change observed in our knockout mice would indicate a 19–23  $\mu$ m axial elongation. The axial length of the WT mouse eye is approximately 3 mm, and it is difficult to obtain statistically significant results based on such a large baseline for such a small absolute alternation. Alternatively, the myopic RE in knockout mice may be attributed to corneal thinning other than elongated axial length<sup>49 50</sup>; (4) although it is evident that *Gla2* knockout decreased rod cell genesis in the mouse retina, the mechanism underlying this phenomenon is unknown. Reduced cell proliferation, increased cell apoptosis and the downstream cascade caused by *Gla2* knockout should be explored.

In summary, this study demonstrated that *GLRA2* is a novel HM-causing gene and revealed the importance of extracellular glycine-gated chloride channels during HM onset and progression. In addition, this study added new evidence to previous suggestions that abnormal visual experience is a driver for HM and that ion channels are involved in this process.<sup>13 20 41</sup> Nonetheless, more efforts should be made to elucidate the detailed HM pathogenic mechanism caused by *GLRA2* mutations.

#### Author affiliations

- <sup>1</sup>Center for Medical Genetics, School of Life Sciences, Central South University, Changsha, Hunan, People's Republic of China
- <sup>2</sup>Hunan Key Laboratory of Medical Genetics, School of Life Sciences, Central South University, Changsha, Hunan, People's Republic of China
- <sup>3</sup>Hunan Key Laboratory of Animal Models for Human Disease, School of Life Sciences, Central South University, Changsha, Hunan, People's Republic of China
- <sup>4</sup>Department of Ophthalmology, The Second Xiangya Hospital, Central South University, Changsha, Hunan, People's Republic of China
- <sup>5</sup>Hunan Province Key Laboratory of Basic and Applied Hematology, School of Life Sciences, Central South University, Changsha, Hunan, People's Republic of China
- <sup>6</sup>Department of Biochemistry and Molecular Biology, School of Life Sciences, Central South University, Changsha, Hunan, People's Republic of China
- <sup>7</sup>Reproductive Center, Sanya Central Hospital, Sanya, Hainan, People's Republic of China

**Acknowledgements** We would like to thank Dr Jieqiong Tan for writing advice.

**Contributors** Conceptualisation: QT, PT, KX, ZH; data curation: QT, RT, MD; formal analysis: QT, TC, GC, MD, RT; funding acquisition: ZH, QT, PT; investigation: QT, TC, GC, MD, RT, ZZ; methodology: QT, TC, GC, MD, RT, ZZ; resources: QT, PT, TC, ZH; supervision: QT, PT, KX, ZH; visualisation: QT, RT, MD; writing-original draft: QT, PT, KX, ZH; writing-review and editing: QT, PT, KX, ZH. ZH acting as guarantor.

**Funding** This study was supported by the Key R&D Program of Hunan Province (grant number 2019SK2051), National Key R&D Program of China (grant number 2021YFA0805200), the Natural Science Foundation of Hunan Province (grant

number 2019JJ70002, 2021JJ40811 and 2021JJ30955), the Natural Science Foundation of Changsha City (grant number kq2014248).

**Competing interests** None declared.

**Patient consent for publication** Not applicable.

**Ethics approval** This study was approved by the Institutional Review Board of the School of Life Sciences, Central South University (2021-1-10). All subjects who participated in this study have thoroughly read and signed the informed consent form before blood samples were collected for further analysis.

**Provenance and peer review** Not commissioned; externally peer reviewed.

**Data availability statement** All data relevant to the study are included in the article or uploaded as supplementary information. Not applicable.

**Supplemental material** This content has been supplied by the author(s). It has not been vetted by BMJ Publishing Group Limited (BMJ) and may not have been peer-reviewed. Any opinions or recommendations discussed are solely those of the author(s) and are not endorsed by BMJ. BMJ disclaims all liability and responsibility arising from any reliance placed on the content. Where the content includes any translated material, BMJ does not warrant the accuracy and reliability of the translations (including but not limited to local regulations, clinical guidelines, terminology, drug names and drug dosages), and is not responsible for any error and/or omissions arising from translation and adaptation or otherwise.

**Open access** This is an open access article distributed in accordance with the Creative Commons Attribution Non Commercial (CC BY-NC 4.0) license, which permits others to distribute, remix, adapt, build upon this work non-commercially, and license their derivative works on different terms, provided the original work is properly cited, appropriate credit is given, any changes made indicated, and the use is non-commercial. See: <http://creativecommons.org/licenses/by-nc/4.0/>.

#### ORCID iDs

Qi Tian <http://orcid.org/0000-0003-0798-2759>

Zhengmao Hu <http://orcid.org/0000-0002-3921-8205>

#### REFERENCES

- 1 Sabanayagam C, Cheng C-Y. Global causes of vision loss in 2015: are we on track to achieve the vision 2020 target? *Lancet Glob Health* 2017;5:e1164–5.
- 2 GBD 2016 Disease and Injury Incidence and Prevalence Collaborators. Global, regional, and national incidence, prevalence, and years lived with disability for 328 diseases and injuries for 195 countries, 1990–2016: a systematic analysis for the global burden of disease study 2016. *Lancet* 2017;390:1211–59.
- 3 Bourne RRA, Stevens GA, White RA, Smith JL, Flaxman SR, Price H, Jonas JB, Keeffe J, Leasher J, Naidoo K, Pesudovs K, Resnikoff S, Taylor HR, Vision Loss Expert Group. Causes of vision loss worldwide, 1990–2010: a systematic analysis. *Lancet Glob Health* 2013;1:e339–49.
- 4 Organization WH. *The impact of myopia and high myopia: report of the joint World Health Organization–Brien Holden vision Institute global scientific meeting on myopia*. Geneva, Switzerland: World Health Organization, 2015.
- 5 Flitcroft DI, He M, Jonas JB, Jong M, Naidoo K, Ohno-Matsui K, Rahi J, Resnikoff S, Vitale S, Yannuzzi L, Defining IMI-IMI - Defining and Classifying Myopia: A Proposed Set of Standards for Clinical and Epidemiologic Studies. *Invest Ophthalmol Vis Sci* 2019;60:M20–30.
- 6 Liu R, Guo X, Xiao O, Li Z, Zhang J, Lee JTL, Wang D, Sankaridurg P, Jong M, He M. Diffuse chorioretinal atrophy in Chinese high myopia: the ZOC-BHVI high myopia cohort study. *Retina* 2020;40:241–8.
- 7 World Health O. *International statistical classification of diseases and related health problems: World Health organization*, 2010.
- 8 Holden BA, Fricke TR, Wilson DA, Jong M, Naidoo KS, Sankaridurg P, Wong TY, Naduvilath TJ, Resnikoff S. Global prevalence of myopia and high myopia and temporal trends from 2000 through 2050. *Ophthalmology* 2016;123:1036–42.
- 9 Kim MH, Zhao D, Kim W, Lim D-H, Song Y-M, Guallar E, Cho J, Sung J, Chung E-S, Chung T-Y. Heritability of myopia and ocular biometrics in Koreans: the healthy twin study. *Invest Ophthalmol Vis Sci* 2013;54:3644–9.
- 10 Williams KM, Hysi P, Hammond CJ. Twin studies, genome-wide association studies and myopia genetics. *Annals of Eye Science* 2017;2.
- 11 Guo H, Tong P, Liu Y, Xia L, Wang T, Tian Q, Li Y, Hu Y, Zheng Y, Jin X, Li Y, Xiong W, Tang B, Feng Y, Li J, Pan Q, Hu Z, Xia K. Mutations of P4HA2 encoding prolyl 4-hydroxylase 2 are associated with nonsyndromic high myopia. *Genet Med* 2015;17:300–6.
- 12 Cai X-B, Shen S-R, Chen D-F, Zhang Q, Jin Z-B. An overview of myopia genetics. *Exp Eye Res* 2019;188:107778.
- 13 Tedja MS, Wojciechowski R, Hysi PG, Eriksson N, Furlotte NA, Verhoeven VJM, Iglesias AI, Meester-Smoor MA, Tompson SW, Fan Q, Khawaja AP, Cheng C-Y, Höhn R, Yamashiro K, Wenocur A, Grazal C, Haller T, Metspalu A, Wedenoja J, Jonas JB, Wang YX, Xie J, Mitchell P, Foster PJ, Klein BEK, Klein R, Paterson AD, Hosseini SM, Shah RL, Williams C, Teo YY, Tham YC, Gupta P, Zhao W, Shi Y, Saw W-Y, Tai E-S, Sim XL, Huffman JE, Polašek O, Hayward C, Bencic G, Rudan I, Wilson JF, Joshi PK, Tsujikawa A, Matsuda F, Whisenhunt KN, Zeller T, van der Spek PJ, Haak R, Meijers-Heijboer

- H, van Leeuwen EM, Iyengar SK, Lass JH, Hofman A, Rivadeneira F, Uitterlinden AG, Vingerling JR, Lehtimäki T, Raitakari OT, Biino G, Concas MP, Schwantes-An T-H, Igo RP, Cuellar-Partida G, Martin NG, Craig JE, Garahkhani P, Williams KM, Nag A, Rahi JS, Cumberland PM, Delcourt C, Bellenguez C, Ried JS, Bergen AA, Meitinger T, Gieger C, Wong TY, Hewitt AW, Mackey DA, Simpson CL, Pfeiffer N, Pärssinen O, Baird PN, Vitart V, Amin N, van Duijn CM, Bailey-Wilson JE, Young TL, Saw S-M, Stambolian D, MacGregor S, Guggenheim JA, Tung JY, Hammond CJ, Klaver CCW, CREAM Consortium, 23andMe Research Team, UK Biobank Eye and Vision Consortium. Genome-Wide association meta-analysis highlights light-induced signaling as a driver for refractive error. *Nat Genet* 2018;50:834–48.
- 14 Forrester JV, Dick AD, McMenamin PG, Roberts F, Pearlman E. Chapter 1 - Anatomy of the eye and orbit. In: Forrester JV, Dick AD, McMenamin PG, Roberts F, Pearlman E, eds. *The eye*. Fourth Edition. W.B. Saunders, 2016: 1–102.
- 15 Tedja MS, Haarman AEG, Meester-Smoor MA, Verhoeven VJM, Klaver CCW, MacGregor S. The Genetics of Myopia. In: Ang M, Wong TY, eds. *Updates on myopia: a clinical perspective*. Singapore: Springer Singapore, 2020: 95–132.
- 16 Harper AR, Summers JA. The dynamic sclera: extracellular matrix remodeling in normal ocular growth and myopia development. *Exp Eye Res* 2015;133:100–11.
- 17 Verhoeven VJM, Hysi PG, Wojciechowski R, Paterson AD, Hysi PG, Guggenheim JA, Höhn R, MacGregor S, Hewitt AW, Nag A, Cheng C-Y, Yonova-Doing E, Zhou X, Ikram MK, Buitendijk GHS, McMahon G, Kemp JP, Pourcain BS, Simpson CL, Mäkelä K-M, Lehtimäki T, Kähönen M, Paterson AD, Hosseini SM, Wong HS, Xu L, Jonas JB, Pärssinen O, Wedenoja J, Yip SP, Ho DW, Pang CP, Chen LJ, Burdon KP, Craig JE, Klein BEK, Klein R, Haller T, Metspalu A, Khor C-C, Tai E-S, Aung T, Vithana E, Tay W-T, Barathi VA, Chen P, Li R, Liao J, Zheng Y, Ong RT, Döring A, Evans DM, Timpson NJ, Verkerk AJMH, Meitinger T, Raitakari O, Hawthorne F, Spector TD, Karssen LC, Pirastu M, Murgia F, Ang W, Mishra A, Montgomery GW, Pennell CE, Cumberland PM, Cotlarciuc I, Mitchell P, Wang JJ, Schache M, Janmahasatian S, Janmahasatian S, Igo RP, Lass JH, Chew E, Iyengar SK, Gorgels TGMF, Rudan I, Hayward C, Wright AF, Polasek O, Vataavuk Z, Wilson JF, Fleck B, Zeller T, Mirshahi A, Müller C, Uitterlinden AG, Rivadeneira F, Vingerling JR, Hofman A, Oostra BA, Amin N, Bergen AAB, Teo Y-Y, Rahi JS, Vitart V, Williams C, Baird PN, Wong T-Y, Oexle K, Pfeiffer N, Mackey DA, Young TL, van Duijn CM, Saw S-M, Bailey-Wilson JE, Stambolian D, Klaver CC, Hammond CJ, Consortium for Refractive Error and Myopia (CREAM), Diabetes Control and Complications Trial/Epidemiology of Diabetes Interventions and Complications (DCCT/EDIC) Research Group, Wellcome Trust Case Control Consortium 2 (WTC2), Fuchs' Genetics Multi-Center Study Group. Genome-Wide meta-analyses of multiethnicity cohorts identify multiple new susceptibility loci for refractive error and myopia. *Nat Genet* 2013;45:314–8.
- 18 Kiefer AK, Tung JY, Do CB, Hinds DA, Mountain JL, Francke U, Eriksson N. Genome-Wide analysis points to roles for extracellular matrix remodeling, the visual cycle, and neuronal development in myopia. *PLoS Genet* 2013;9:e1003299.
- 19 Hysi PG, Wojciechowski R, Rahi JS, Hammond CJ. Genome-Wide association studies of refractive error and myopia, lessons learned, and implications for the future. *Invest Ophthalmol Vis Sci* 2014;55:3344–51.
- 20 Hysi PG, Choquet H, Khawaja AP, Wojciechowski R, Tedja MS, Yin J, Simcoe MJ, Patasova K, Mahroo OA, Thai KK, Cumberland PM, Melles RB, Verhoeven VJM, Vitart V, Segre A, Stone RA, Wareham N, Hewitt AW, Mackey DA, Klaver CCW, MacGregor S, Khaw PT, Foster PJ, Guggenheim JA, Rahi JS, Jorgenson E, Hammond CJ, Consortium for Refractive Error and Myopia, UK Eye and Vision Consortium, 23andMe Inc. Meta-Analysis of 542,934 subjects of European ancestry identifies new genes and mechanisms predisposing to refractive error and myopia. *Nat Genet* 2020;52:401–7.
- 21 Fan Q, Guo X, Tideman JW, Williams KM, Yazar S, Hosseini SM, Howe LD, Pourcain BS, Evans DM, Timpson NJ, McMahon G, Hysi PG, Krapohl E, Wang YX, Jonas JB, Baird PN, Wang JJ, Cheng C-Y, Teo Y-Y, Wong T-Y, Ding X, Wojciechowski R, Young TL, Pärssinen O, Oexle K, Pfeiffer N, Bailey-Wilson JE, Paterson AD, Klaver CCW, Plomin R, Hammond CJ, Mackey DA, He M, Saw S-M, Williams C, Guggenheim JA, Consortium C, CREAM Consortium. Childhood gene-environment interactions and age-dependent effects of genetic variants associated with refractive error and myopia: the cream Consortium. *Sci Rep* 2016;6:25853.
- 22 Li J, Gao B, Guan L, Xiao X, Zhang J, Li S, Jiang H, Jia X, Yang J, Guo X, Yin Y, Wang J, Zhang Q. Unique variants in OPN1LW cause both syndromic and nonsyndromic X-linked high myopia mapped to myp1. *Invest Ophthalmol Vis Sci* 2015;56:4150–5.
- 23 Yip SP, Li CC, Yiu WC, Hung WH, Lam WW, Lai MC, Ng PW, Fung WY, Chu PHW, Jiang B, Chan HHL, Yap MKH. A novel missense mutation in the NYX gene associated with high myopia. *Ophthalmic Physiol Opt* 2013;33:346–53.
- 24 Troilo D, Smith EL, Nickla DL, Ashby R, Tkatchenko AV, Ostrin LA, Gawne TJ, Pardue MT, Summers JA, Kee C-S, Schroedel F, Wahl S, Jones L. IMI - Report on Experimental Models of Emmetropization and Myopia. *Invest Ophthalmol Vis Sci* 2019;60:M31–88.
- 25 Carr BJ, Stell WK. The science behind myopia. In: Kolb H, Fernandez E, Nelson R, eds. *Webvision: the organization of the retina and visual system*. Salt Lake City (UT), 1995.
- 26 Abecasis GR, Cherny SS, Cookson WO, Cardon LR. Merlin-rapid analysis of dense genetic maps using sparse gene flow trees. *Nat Genet* 2002;30:97–101.
- 27 Tian Q, Li Y, Kousar R, Guo H, Peng F, Zheng Y, Yang X, Long Z, Tian R, Xia K, Lin H, Pan Q. A novel NHS mutation causes Nance-Horan syndrome in a Chinese family. *BMC Med Genet* 2017;18:2.
- 28 Li H, Durbin R. Fast and accurate long-read alignment with Burrows-Wheeler transform. *Bioinformatics* 2010;26:589–95.
- 29 Van der Auwera GA, Carneiro MO, Hartl C, Poplin R, Del Angel G, Levy-Moonshine A, Jordan T, Shaker K, Roazen D, Thibault J, Banks E, Garimella KV, Altshuler D, Gabriel S, DePristo MA. From FastQ data to high confidence variant calls: the genome analysis toolkit best practices pipeline. *Curr Protoc Bioinformatics* 2013;43.
- 30 Wang K, Li M, Hakonarson H. ANNOVAR: functional annotation of genetic variants from high-throughput sequencing data. *Nucleic Acids Res* 2010;38:e164.
- 31 Prusky GT, West PW, Douglas RM. Behavioral assessment of visual acuity in mice and rats. *Vision Res* 2000;40:2201–9.
- 32 Schaeffel F, Burkhardt E, Howland HC, Williams RW. Measurement of refractive state and deprivation myopia in two strains of mice. *Optom Vis Sci* 2004;81:99–110.
- 33 Zhou X, Xie J, Shen M, Wang J, Jiang L, Qu J, Lu F. Biometric measurement of the mouse eye using optical coherence tomography with focal plane advancement. *Vision Res* 2008;48:1137–43.
- 34 Zhang Y, Ho TNT, Harvey RJ, Lynch JW, Keramidis A. Structure-Function analysis of the GlyR  $\alpha 2$  subunit autism mutation p.R323L reveals a gain-of-function. *Front Mol Neurosci* 2017;10:158.
- 35 Pilorge M, Fassier C, Le Corronc H, Potey A, Bai J, De Gois S, Delaby E, Assouline B, Guinchat V, Devillard F, Delorme R, Nygren G, Råstam M, Meier JC, Otani S, Cheval H, James VM, Topf M, Dear TN, Gillberg C, Leboyer M, Giros B, Gautron S, Hazan J, Harvey RJ, Legendre P, Betancur C. Genetic and functional analyses demonstrate a role for abnormal glycinergic signaling in autism. *Mol Psychiatry* 2016;21:936–45.
- 36 Malosio ML, Marqu e-Pouey B, Kuhse J, Betz H. Widespread expression of glycine receptor subunit mRNAs in the adult and developing rat brain. *Embo J* 1991;10:2401–9.
- 37 Jusuf PR, Haverkamp S, Gr nert U. Localization of glycine receptor alpha subunits on bipolar and amacrine cells in primate retina. *J Comp Neurol* 2005;488:113–28.
- 38 Nobles RD, Zhang C, M ller U, Betz H, McCall MA. Selective glycine receptor  $\alpha 2$  subunit control of crossover inhibition between the on and off retinal pathways. *J Neurosci* 2012;32:3321–32.
- 39 Liang Z, Freed MA. Cross inhibition from on to off pathway improves the efficiency of contrast encoding in the mammalian retina. *J Neurophysiol* 2012;108:2679–88.
- 40 Young TL, Cepko CL. A role for ligand-gated ion channels in rod photoreceptor development. *Neuron* 2004;41:867–79.
- 41 Hysi PG, Mahroo OA, Cumberland P, Wojciechowski R, Williams KM, Young TL, Mackey DA, Rahi JS, Hammond CJ. Common mechanisms underlying refractive error identified in functional analysis of gene lists from genome-wide association study results in 2 European British cohorts. *JAMA Ophthalmol* 2014;132:50–6.
- 42 Huang X, Chen H, Michelsen K, Schneider S, Shaffer PL. Crystal structure of human glycine receptor- $\alpha 3$  bound to antagonist strychnine. *Nature* 2015;526:277–80.
- 43 Rajendra S, Vandenberg RJ, Pierce KD, Cunningham AM, French PW, Barry PH, Schofield PR. The unique extracellular disulfide loop of the glycine receptor is a principal ligand binding element. *Embo J* 1995;14:2987–98.
- 44 Beato M. The time course of transmitter at glycinergic synapses onto motoneurons. *J Neurosci* 2008;28:7412–25.
- 45 Pinto D, Pagnamenta AT, Klei L, Anney R, Merico D, Regan R, Conroy J, Magalhaes TR, Correia C, Abrahams BS, Almeida J, Bacchelli E, Bader GD, Bailey AJ, Baird G, Battaglia A, Berney T, Bolshakova N, B lte S, Bolton PF, Bourgeron T, Brennan S, Brian J, Bryson SE, Carson AR, Casallo G, Casey J, Chung BHY, Cochrane L, Corsello C, Crawford EL, Crossett A, Cytrynbaum C, Dawson G, de Jonge M, Delorme R, Drmic I, Duketis E, Duque F, Estes A, Farrar P, Fernandez BA, Folstein E, Fombonne E, Freitag CM, Gilbert J, Gillberg C, Glessner JT, Goldberg J, Green A, Green J, Guter SJ, Hakonarson H, Heron EA, Hill M, Holt R, Howe JL, Hughes G, Hus V, Iglizoi R, Kim C, Klauk SM, Kolevzon A, Korvatska O, Kustanovich V, Lajonchere CM, Lamb JA, Laskawiec M, Leboyer M, Le Couteur A, Leventhal BL, Lionel AC, Liu X-Q, Lord C, Lotspeich L, Lund SC, Maestrini E, Mahoney W, Mantoulan C, Marshall CR, McConachie H, McDougle CJ, McGrath J, McMahon WM, Merikangas A, Migita O, Minschew NJ, Mirza GK, Munson J, Nelson SF, Noakes C, Noor A, Nygren G, Oliveira G, Papanikolaou K, Parr JR, Parrini B, Paton T, Pickles A, Pilorge M, Piven J, Ponting CP, Popy NJ, Poustka A, Poustka F, Prasad A, Ragoussis J, Renshaw K, Rickaby J, Roberts W, Roeder K, Roge B, Rutter ML, Bierut LJ, Rice JP, Salt J, Sansom K, Sato D, Segurado R, Sequeira AF, Senman L, Shah N, Sheffield VC, Soorya L, Sousa I, Stein O, Sykes N, Stoppioni V, Strawbridge C, Tancredi R, Tansey K, Thiruvahindrapuram B, Thompson AP, Thomson S, Tryfan A, Tsiantis J, Van Engeland H, Vincent JB, Volkmar F, Wallace S, Wang K, Wang Z, Wassink TH, Webber C, Weksberg R, Wing K, Wittmeyer K, Wood S, Wu J, Yaspan BL, Zurawiecki D, Zwaigenbaum L, Buxbaum JD, Cantor RM, Cook EH, Cooch H, Cuccaro ML, Devlin B, Ennis S, Gallagher L, Geschwind DH, Gill M, Haines JL, Hallmayer J, Miller J, Monaco AP, Nurnberger JI, Paterson AD, Pericak-Vance MA, Schellenberg GD, Szatmari P, Vicente AM, Vieland VJ, Wijsman EM, Scherer SW, Sutcliffe JS, Betancur C. Functional impact of global rare copy number variation in autism spectrum disorders. *Nature* 2010;466:368–72.
- 46 Piton A, Gauthier J, Hamdan FF, Lafreni re RG, Yang Y, Henrion E, Laurent S, Noreau A, Thibodeau P, Karamera L, Spiegelman D, Kuku F, Duguay J, Destroisaisons L, Jolivet P, C t  M, Lachapelle K, Diallo O, Raymond A, Marineau C, Champagne N, Xiong L, Gaspar C, Riviere J-B, Tarabeux J, Cossette P, Krebs M-O, Rapoport JL, Addington A, Delisi LE, Mottron L, Joobler R, Fombonne E, Drapeau P, Rouleau GA. Systematic resequencing of X-chromosome synaptic genes in autism spectrum disorder and schizophrenia. *Mol Psychiatry* 2011;16:867–80.

- 47 Iossifov I, O’Roak BJ, Sanders SJ, Ronemus M, Krumm N, Levy D, Stessman HA, Witherspoon KT, Vives L, Patterson KE, Smith JD, Paeper B, Nickerson DA, Dea J, Dong S, Gonzalez LE, Mandell JD, Mane SM, Murtha MT, Sullivan CA, Walker MF, Waqar Z, Wei L, Willsey AJ, Yamrom B, Lee Y-ha, Grabowska E, Dalkic E, Wang Z, Marks S, Andrews P, Leotta A, Kendall J, Hakker I, Rosenbaum J, Ma B, Rodgers L, Troge J, Narzisi G, Yoon S, Schatz MC, Ye K, McCombie WR, Shendure J, Eichler EE, State MW, Wigler M. The contribution of de novo coding mutations to autism spectrum disorder. *Nature* 2014;515:216–21.
- 48 Schmucker C, Schaeffel F. A paraxial schematic eye model for the growing C57BL/6 mouse. *Vision Res* 2004;44:1857–67.
- 49 Pedersen L, Hjortdal J, Ehlers N. Central corneal thickness in high myopia. *Acta Ophthalmol Scand* 2005;83:539–42.
- 50 Uçakhan OO, Gesoğlu P, Ozkan M, Kanpolat A. Corneal elevation and thickness in relation to the refractive status measured with the Pentacam scheinplufug system. *J Cataract Refract Surg* 2008;34:1900–5.